

Effects of the difference between the charge and matter deformations on fusion reactions of unstable nuclei

Tamanna Rumin ^{*} and Noboru Takigawa, [†]

Department of Physics, Tohoku University, Sendai 980-8578, Japan

(November 10, 2018)

Relativistic mean field calculations suggest that the charge and matter deformations significantly differ in some of the unstable neutron and proton rich nuclei. We discuss the effects of the difference on the fusion reactions induced by them at energies near and below the Coulomb barrier by taking the $^{19,25,37}\text{Na} + ^{208}\text{Pb}$ reactions as examples. We also discuss whether one can probe the difference by the so called fusion barrier distribution analysis.

21.65.+f, 24.10.Eq, 24.10.Jv, 25.60.Pj

I. INTRODUCTION

Secondary beam experiments are opening up new physics to be studied for a variety of unstable nuclei across the beta-stability line in the nuclear chart. One of the basic questions is to study their charge and matter deformations. We are especially interested in the difference between the charge and matter deformations in each unstable nucleus. One cannot, however, apply the standard techniques such as the gamma ray spectroscopy which have been used for stable nuclei. A possibility is to use heavy-ion fusion reactions at energies below or near the Coulomb barrier, which have recently been established to be very sensitive to the shape of the target and/or projectile nuclei [1,2]. An alternative is to predict the charge and matter deformations theoretically based on the non-relativistic Hartree Fock or the relativistic mean field calculations with various refinements such as including the pairing correlations.

In this paper, we take Na isotopes as an example to anticipate the variation of the charge and matter deformations along an isotope chain and discuss whether the significant difference between them expected for some isotopes can be probed through the analysis of the fusion reactions induced by them by assuming ^{208}Pb as the target nucleus. We use the relativistic mean field calculations to assess the charge and matter deformations for each Na isotope. We then calculate the fusion cross section $\sigma(E)$ based on the coupled-channels formalism assuming thus obtained values of deformations and taking the ground state rotational band into account. We then calculate the associated so called fusion barrier distribution $\frac{d^2(E\sigma(E))}{dE^2}$ [3].

The paper is organized as follows. In sect.2 we describe the formalism of our coupled-channels calculations, i.e. the simplified framework based on the no-Coriolis approximation, somewhat in detail, because the formalism is not well known for the case of fusion of a deformed odd mass projectile which we are going to discuss in this paper. In sect. 3, we present the results of the relativistic mean field calculations and of the coupled-channels analyses. The paper is summarized in sect.4.

II. SIMPLIFIED COUPLED-CHANNELS FORMALISM FOR THE FUSION OF A DEFORMED ODD-MASS NUCLEUS

We discuss in the next section the fusion of deformed odd mass Na isotopes with ^{208}Pb target. We calculate the fusion cross section by taking the excitation of the ground state rotational band of the Na projectile into account with the coupled-channels formalism in the no-Coriolis approximation. In this section, we describe the major aspects of the method.

We denote the coordinates of the relative motion between the projectile and target nuclei and of the rotational motion of the projectile, i.e. a Na isotope, by \vec{R} and $\hat{\xi}$, respectively. We ignore the intrinsic excitation of ^{208}Pb . The total Hamiltonian is then given by

^{*}Electronic address: rumin@nucl.phys.tohoku.ac.jp

[†]Electronic address: takigawa@nucl.phys.tohoku.ac.jp

$$H(\vec{R}, \xi) = \hat{T}_R + V_0(R) + H_0(\xi) + V(\vec{R}, \xi) \quad (1)$$

with

$$\hat{T}_R = -\frac{\hbar^2}{2\mu} \frac{1}{R^2} \frac{d}{dR} R^2 \frac{d}{dR} + \frac{\hbar^2}{2\mu R^2} \hat{L}^2$$

$V_0(R)$ is the sum of monopole nuclear and Coulomb interactions between the projectile and target nuclei. We call it the bare interaction. $H_0(\xi)$ is the intrinsic Hamiltonian of each Na projectile, whose eigenfunctions and the eigenvalues are denoted as $\varphi_{Im_I}^K(\xi)$ and ϵ_{IK} ,

$$H_0(\xi) \varphi_{Im_I}^K(\xi) = \epsilon_{IK} \varphi_{Im_I}^K(\xi) \quad (2)$$

We assume that each deformed Na isotope can be well described by the strong coupling model [4] for the rotational excitation, where the wave function is given by

$$\varphi_{Im_I}^K(\xi) = \sqrt{\frac{2I+1}{16\pi^2}} \left\{ D_{m_I K}^I(\Omega) \chi_K + (-1)^{I+K} D_{m_I -K}^I(\Omega) \chi_{-K} \right\} \quad (3)$$

On the r.h.s. of eq.(3), we used Ω for ξ in order to explicitly indicate the physical meaning as the Euler angles. χ_K is the intrinsic wave function. We assume the deformation to be axially symmetric, and K is the component of the angular momentum of the rotational motion along the symmetry axis.

The $V(\vec{R}, \xi)$ in eq.(1) represents the interaction between the projectile and target nuclei after the monopole part has been subtracted. We assume the same form of coupling Hamiltonian as that is familiar in coupled-channels calculations for the fusion reactions of even-even nuclei. It consists of the nuclear and Coulomb parts, and is expressed as

$$V(\vec{R}, \xi) = f^N(R) \sum_{\lambda} Y_{\lambda}(\hat{R}) \cdot T_{\lambda}(\xi) + \sum_{\lambda\mu} f_{\lambda}^C(R) Y_{\lambda\mu}(\hat{R}) T_{\lambda\mu}^*(\xi) \quad (4)$$

in terms of the spherical harmonics for the relative motion and the tensor operators $\hat{T}_{\lambda\mu}$ which cause the rotational excitation of the Na projectile. We further assume the latter to be given by

$$T_{\lambda\mu}(\xi) = \sum_{\nu} a_{\lambda\nu} \mathcal{D}_{\mu\nu}^{\lambda}(\Omega) = a_{\lambda 0} \mathcal{D}_{\mu 0}^{\lambda}(\Omega) = \beta_{\lambda} \mathcal{D}_{\mu 0}^{\lambda}(\Omega) \quad (5)$$

where $a_{\lambda\nu}$ are the deformation parameters in the body fixed frame [4]. We have kept only the $\nu = 0$ term to be consistent with the assumption of the axially symmetric deformation. The deformation parameter β_{λ} is identified with the nuclear and the charge deformation parameters, β_{λ}^N and β_{λ}^C , in the nuclear and Coulomb coupling terms, respectively. The $f^N(R)$ and $f_{\lambda}^C(R)$ are the nuclear and Coulomb coupling form factors, which we assume to be,

$$f^N(R) = -R_P \frac{d}{dR} \left[\frac{-V_0}{1 + \exp[R - R_0]/a_0} \right], \quad f_{\lambda}^C(R) = \frac{3Z_P Z_T e^2}{2\lambda + 1} \frac{R_P^{\lambda}}{R^{\lambda+1}}$$

with $R_0 = R_P + R_T$, R_P and R_T being the nuclear radii of the projectile and target.

As usual, we introduce the channel wave functions by

$$\phi_{IKL}^{JM}(\hat{R}, \xi) = \sum_{m_L m_I} (L m_L I m_I | JM) Y_{L m_L}(\hat{R}) \varphi_{Im_I}^K(\xi) \quad (6)$$

and expand the total wave function for a fixed total angular momentum J and its z component M as,

$$\Psi^{JM}(\vec{R}, \xi) = \sum_{IKL} \frac{1}{R} \Phi_{IKL}^J(R) \phi_{IKL}^{JM}(\hat{R}, \xi) \quad (7)$$

It is then straight-forward to obtain the following coupled 2nd order differential equations which determine the radial wave functions of the relative motion $\Phi_{IKL}^J(R)$,

$$\left[-\frac{\hbar^2}{2\mu} \frac{d^2}{dR^2} + V_0(R) + \frac{\hbar^2}{2\mu R^2} L(L+1) + \epsilon_{IK} - E \right] \Phi_{IKL}^J(R) + \sum_{\lambda' K' L'} V_{IKL, I' K' L'}(R) \Phi_{I' K' L'}^J(R) = 0 \quad (8)$$

where the coupling matrix elements are given by

$$V_{IKL, I'K'L'}(R) = \left[f^N(R) \beta_\lambda^N + f_\lambda^C(R) \beta_\lambda^C \right] (-1)^{L+J+L'+I'} \left[\frac{1+(-1)^\lambda}{2} \right] \sqrt{\frac{(2I'+1)(2L+1)(2\lambda+1)(2L'+1)}{4\pi}} \begin{pmatrix} L & \lambda & L' \\ 0 & 0 & 0 \end{pmatrix} \left\{ \begin{array}{ccc} L & I & J \\ I' & L' & \lambda \end{array} \right\} (\lambda 0 I' K | I K) \delta_{KK'} \quad (9)$$

In obtaining eq.(8) with eq.(9), we used the explicit expression of the tensor operator $T_{\lambda\mu}$ given by eq.(5), which leads to the selection rule $\delta_{KK'}$.

The full coupled-channels equations (8) become fairly intricate if many channels are included. In this paper, we use the no-Coriolis approximation, in other words the rotating frame approximation, which considerably reduces the dimension of the coupled equations [5]. The process to calculate the fusion cross section then consists of three major steps. The first is to replace the channel dependent centrifugal potential energy in eq.(8) by that in the entrance channel,

$$\frac{L(L+1)\hbar^2}{2\mu R^2} \approx \frac{L_i(L_i+1)\hbar^2}{2\mu R^2} \quad (10)$$

where L_i is the initial orbital angular momentum.

The second step is to perform the unitary transformation,

$$\tilde{\Phi}_{I\tilde{K}}^{JK}(R) = \sum_L \sqrt{\frac{2L+1}{2J+1}} (L 0 I \tilde{K} | J \tilde{K}) \Phi_{IKL}^J(R) \quad (11)$$

which transforms the original coupled-channels equations eq.(8) into

$$\left[-\frac{\hbar^2}{2\mu} \frac{d^2}{dR^2} + V_0(R) + \frac{L_i(L_i+1)\hbar^2}{2\mu R^2} + \epsilon_{IK} - E \right] \tilde{\Phi}_{I\tilde{K}}^{JK}(R) + \sum_{\lambda I'} V'_{I\tilde{K}, I'\tilde{K}}(R) \tilde{\Phi}_{I'\tilde{K}}^{JK}(R) = 0 \quad (12)$$

with

$$V'_{I\tilde{K}, I'\tilde{K}}(R) = (-1)^{I+2\lambda-I'} \left[f^N(R) \beta_\lambda^N + f_\lambda^C(R) \beta_\lambda^C \right] \left[\frac{1+(-1)^\lambda}{2} \right] \sqrt{\frac{(2\lambda+1)(2I'+1)}{4\pi(2I+1)}} (\lambda 0 I' K | I K) (\lambda 0 I' - \tilde{K} | I - \tilde{K}) \quad (13)$$

The \tilde{K} is the projection of the intrinsic spin of the Na projectile along the z-axis of the rotating frame which is taken to be parallel to \vec{R} . Eq.(12) shows that only states with the same \tilde{K} quantum number couple to each other. The dimension of the coupled-channels equations is thus considerably reduced.

The third step is to solve the reduced coupled-channels equations for each $\tilde{K} = -I_i, -I_i + 1, \dots, I_i - 1, I_i, I_i$ being the ground state spin of the Na projectile. Note that $K = I_i$ is fixed. As usually done for heavy-ion fusion reactions, we replace the proper boundary condition that the radial wave functions for the relative motion should be regular at the origin $R = 0$ by the incoming wave boundary condition at an absorption radius R_{abs} inside the potential pocket, and require

$$\tilde{\Phi}_{I\tilde{K}}^{JK}(R) \sim \begin{cases} T_{I\tilde{K}}^{L_i K} \exp \left[-i \int_{R_{abs}}^R (k_{L_i I K \tilde{K}}(R')) dR' \right], & R \leq R_{abs} \\ H_J^-(k_{IK} R) \delta_{II_i} + R_{I\tilde{K}}^{L_i K} H_J^+(k_{IK} R), & R \rightarrow \infty \end{cases} \quad (14)$$

with

$$k_{IK} = \sqrt{2\mu/\hbar^2(E - \epsilon_{IK})} \quad (15)$$

$$k_{L_i I K \tilde{K}}(R) = \sqrt{\frac{2\mu}{\hbar^2} \left(E - \epsilon_{IK} - \frac{L_i(L_i+1)\hbar^2}{2\mu R^2} - V_0(R) - V'_{I\tilde{K}, I'\tilde{K}}(R) \right)} \quad (16)$$

In eq.(14), $T_{I\tilde{K}}^{L_i K}$ and $R_{I\tilde{K}}^{L_i K}$ are the transmission and reflection coefficients, respectively. We used these notations instead of $T_{I\tilde{K}}^{JK}$ and $R_{I\tilde{K}}^{JK}$ because all the transmission and the reflection coefficients are the same for a given L_i irrespective of J . Once they are determined, the barrier transmission probability is given by

$$P^{J\tilde{K}}(E) = P^{(J)L_i\tilde{K}}(E) = \sum_I \frac{k_{L_i I K \tilde{K}}}{k} \left| T_{I \tilde{K}}^{L_i K} \right|^2 \quad (17)$$

where $k = k_{I_i K}$ is the wave number in the entrance channel. The first equality in eq.(17) means that the barrier transmission probability is the same for all J for a given L_i .

The fusion cross section can be related to $P^{(J)L_i\tilde{K}}$ by calculating the flux at R_{abs} . To that end, we use the inverse transform of eq.(11),

$$\Phi_{I K L}^J(R) = \sqrt{\frac{2L+1}{2J+1}} \sum_{\tilde{K}} (L 0 I \tilde{K} | J \tilde{K}) \tilde{\Phi}_{I \tilde{K}}^{J K}(R). \quad (18)$$

Averaging over the initial and summing over the final spin projections, we obtain

$$\sigma_f(E) = \frac{\pi}{k^2} \frac{1}{2I_i + 1} \sum_{\tilde{K}, L_i} \sum_{J=L_i - I_i}^{L_i + I_i} (2J + 1) P^{(J)L_i\tilde{K}}(E) \quad (19)$$

$$= \frac{\pi}{k^2} \sum_{\tilde{K}, L_i} (2L_i + 1) P^{L_i\tilde{K}}(E) \quad (20)$$

We have used a simplified notation $P^{L_i\tilde{K}}(E)$ in eq.(20) because what one actually does is to solve the coupled equations eq.(12) for each set of \tilde{K} and L_i and determine the barrier transmission probability. Eq.(20) reduces to the well known formula

$$\sigma_f(E) = \frac{\pi}{k^2} \sum_J (2J + 1) P^J(E)$$

for the fusion between two even-even nuclei by setting the initial intrinsic spin I_i to be zero.

III. THE CHARGE AND MATTER DEFORMATIONS OF NA ISOTOPES AND THEIR EFFECTS ON THE FUSION REACTION

We now discuss the charge and matter deformations of Na isotopes and the influence of their difference on fusion reactions taking $^{19,25,37}\text{Na} + ^{208}\text{Pb}$ scattering as examples. We perform the relativistic mean field (rmf) calculations with the NLSH parameters [6,7] to learn the r.m.s. radii and deformation parameters of the neutron, proton, charge and matter distributions of Na isotopes. Though the pairing correlation may strongly influence the accurate values of deformation [8], we ignore it, because our interest in this paper is to discuss global behaviors. The results are shown in Fig.1, where the solid circles, solid squares and solid triangles represent the r.m.s. radii of the proton, matter and charge distributions, respectively. The open diamonds are the effective root mean square matter radii deduced from the measured interaction cross section using a Glauber-type calculation [9]. We see that the theoretical results given by the solid squares well follow the general trend of the experimental data given by the open diamonds. Fig.1(b) shows the isotope variation of the quadrupole deformation parameters of the proton, matter and neutron distributions. It indicates that the charge and matter deformations are significantly different for many isotopes far away from the beta stability line.

We now discuss how this difference influences the fusion reactions, or conversely whether one can probe this difference through the analysis of the fusion cross section. We choose the $^{19,25,37}\text{Na}$ isotopes as representatives and analyze their fusion reactions with the ^{208}Pb target. As already mentioned, we treat ^{208}Pb as a structureless particle.

Before discussing the results of the coupled-channels calculations, we show in Fig.2 the potential barriers corresponding to fixed orientations of the deformed Na projectile assuming the quadrupole coupling, i.e. $\lambda = 2$,

$$V(R, \theta) = \frac{-V_0}{1 + \exp[(R - R_0 - R_P \beta_2^N \sqrt{\frac{5}{4\pi}} P_2(\cos\theta))/a_0]} + \frac{Z_P Z_T e^2}{R} + \beta_2^C \sqrt{\frac{5}{4\pi}} f_2^C(R) P_2(\cos\theta) \quad (21)$$

where the potential parameters are assumed to be $(V_0, a_0) = (114.2 \text{MeV}, 1.222 \text{fm})$. The radius parameters R_P and R_T have been calculated from the r.m.s. radius given by the rmf calculations according to $R_P(R_T) = \sqrt{\frac{5}{3}} \times \text{r.m.s. radius of the projectile(target)}$. The higher and lower barriers in Fig.2 are for 70.12 and 30.55 degrees, respectively. These

are the effective angles in the so called orientation average formalism in the degenerate spectrum limit approximation when one discusses the effects of the ground state rotational band on the fusion of a deformed even-even nucleus by truncating at the first excited 2^+ state [10]. The dotted line is the potential barrier when the effect of deformation is ignored. For each angle, the solid line is the potential barrier obtained by using different nuclear and Coulomb deformation parameters suggested by the relativistic mean field calculations. It is compared with the dashed line, which has been obtained by ignoring the difference between the charge and matter deformations. It is interesting to observe that the difference of the matter and charge deformations modify the barriers in opposite directions for proton and neutron rich isotopes.

We now present the results of the coupled-channels calculations. There are no experimental data yet on the excited states of $^{19,25,37}\text{Na}$ isotopes. As we stated before, we assume a strong coupling rotational model, where the K quantum number is assigned to be $K=\frac{3}{2}$ for all of them from the Nilsson diagram using the deformations suggested by the relativistic mean field calculations. The excitation energy is given by

$$\epsilon_{IK} = \frac{[I(I+1) - K^2]\hbar^2}{2\mathcal{J}} \quad (22)$$

where \mathcal{J} is the moment of inertia.

It is known that the experimental moment of inertia is smaller than the rigid body value \mathcal{J}_{rig} by about a factor of 2 [4]. Though the deviation of the moment of inertia from the rigid body value is somewhat smaller for odd mass nuclei [4], we assume,

$$\mathcal{J} \approx \mathcal{J}_{rig}/2 \quad (23)$$

for the moment of inertia of $^{19,25,37}\text{Na}$ nuclei. The rigid body value is given by

$$\mathcal{J}_{rig} = \frac{2}{5}AMR^2(1 + \frac{1}{3}\delta) \quad (24)$$

where δ is the deformation parameter, which is related to the quadrupole deformation parameter β_2 as

$$\delta = 0.945\beta_2[1 - \frac{4}{3}\pi^2(a_0/R_P)^2] + 0.34\beta_2^2. \quad (25)$$

In eq. (25), the correction due to the surface diffuseness given through the diffuseness parameter a_0 has been included only to the leading order. The quadrupole deformation parameter β_2 is identified with the matter(nuclear) deformation parameter β_2^N of the Na isotopes.

We solve the coupled-channels equations taking up to the $I_{max}=7/2$ member of the ground state rotational band and including only quadrupole deformation for all three reactions. The fusion cross section is then obtained by eq. (20). Once the fusion excitation function has been obtained, the fusion barrier distribution is calculated by the point difference formula of $\Delta E=2\text{MeV}$ in the center of mass energy. The results are shown in Fig.3. Each figure contains three theoretical lines. The dotted line has been obtained by the potential model. The solid line has been obtained by the coupled channels calculations using the charge and matter deformation parameters obtained from the relativistic mean field calculations. The dashed line has been obtained in the same way, but by ignoring the difference between the charge and matter deformations. We used the value of β^N for both nuclear and charge deformations in this case.

These figures show that the effects of the difference between the charge and matter deformations are significant in the $^{37}\text{Na} + ^{208}\text{Pb}$ fusion reactions. They are noticeable also in the $^{19}\text{Na} + ^{208}\text{Pb}$ fusion reactions. The existence of three or more peaks can be expected because of the truncation at $I_{max}=7/2$ by considering the degenerate spectrum limit. There appear indeed three separated peaks for the $^{37}\text{Na} + ^{208}\text{Pb}$ reaction. The shift of the highest and lowest peak positions by the difference between the charge and matter deformations accords with that shown in Fig.2 for the two channel problem. Unfortunately, no visible effects are seen for the $^{25}\text{Na} + ^{208}\text{Pb}$ fusion reactions, which would be much more tractable experimentally than the other reactions. Though ^{25}Na has a large difference in the charge and matter deformations comparable to that in ^{19}Na and ^{37}Na , its effect on the fusion cross section is compensated by the counter effect of the difference between the charge and matter radii.

The above conclusions might depend on the special choice of the moment of inertia given by eq.(23). In order to test this, we repeat the same calculations for $^{19,37}\text{Na} + ^{208}\text{Pb}$ reactions by changing the moment of inertia to

$$\mathcal{J} \approx \mathcal{J}_{rig}/3 \quad (26)$$

In Fig. 4, the dashed and the solid lines are the same as those in Fig.3 obtained by assuming eq. (23). These lines are compared with the short dashed and the dash-dotted lines which have been obtained by assuming eq. (26). The figures show that the fusion barrier distribution distinguishes the different choice of the moment of inertia and that it clearly reflects the difference of the charge and matter deformations for both choices of the moment of inertia.

IV. SUMMARY

The isotope variation of the charge and matter deformations is an interesting question, which will be addressed with the advent of secondary beam experiments. In this paper, we used relativistic mean field calculations to suggest that the charge and matter deformations can significantly differ from each other for some nuclei far away from the beta stability line. We then performed coupled-channels calculations using these informations, and have shown that the fusion excitation function and the fusion barrier distributions noticeably reflect the difference between the matter and the charge deformations in $^{19,37}\text{Na} + ^{208}\text{Pb}$ reactions. Unfortunately, this effect is compensated by the opposite effect of the difference between the matter and charge radii in the $^{25}\text{Na} + ^{208}\text{Pb}$ fusion reactions which will be more easily tractable experimentally.

Finally, we wish to make some comments on the limitations of our relativistic mean field calculations. We ignored the pairing correlation in our relativistic mean field calculations of Na isotopes. The bulk properties of the light nuclei through helium to oxygen has been calculated by the relativistic mean field theory with and without pairing correlation [11]. The study shows that the r.m.s. radii of light nuclei are not so sensitive to pairing correlation, whereas the deformation parameters are affected considerably. We are now extending the relativistic mean field calculations to include the effects of pairing correlation in order to have a more reliable estimate of the deformation parameters.

ACKNOWLEDGEMENTS

This work is supported by the Grand-in-Aid for Scientific Research from Ministry of Education, Culture, Sports, Science and Technology under Grant No. 12047203 and No. 13640253.

- [1] A.B. Balantekin and N. Takigawa, Rev. of Mod. Phys. **70**, 77 (1998); and references therein.
- [2] M. Dasgupta, D.J. Hinde, N. Rowley and A.M. Stefanini, Annu. Rev. Nucl. Part. Sci., 48, 401(1998); and references therein.
- [3] N. Rowley, G.R. Satchler and P.H. Stelson, Phys. Lett. **B254**, 25 (1991).
- [4] A. Bohr and B.R. Mottelson, Nuclear Structure Vol. II, (Benjamin, London, 1975).
- [5] N. Takigawa and K. Ikeda, in Proceedings of the Symposium on The Many Facets of Heavy Ion Fusion Reactions, Argonne National Laboratory Report No. ANL-PHY- 87-1, 1986, p.613.
- [6] Y.K. Gambhir, P. Ring and A. Thimet, Ann. Phys. **A198**, 132 (1990).
- [7] M.M. Sharma, M.A. Nagarajan and P. Ring, Phys. Lett. **B312**, 377 (1993).
- [8] S. Yoshida and N. Takigawa, Phys. Rev. C55, 1255 (1997).
- [9] T. Suzuki, H. Geissel, O. Bochkarev, L. Chulkov, M. Golovkov, N. Fukunishi, D. Hirata, H. Irnich, Z. Janas, H. Keller, T. Kobayashi, G. Kraus, G. Müzenberg, S. Neumaier, F. Nickel, A. Ozawa, A. Piechaczeck, E. Roeckl, W. Schwab, K. Sümerer, K. Yoshida and I. Tanihata, Nucl. Phys. A630, 661 (1998).
- [10] M.A. Nagarajan, A.B. Balantekin and N. Takigawa, Phys. Rev. C **34**, 894 (1986).
- [11] S.K. Patra, Phys. Rev. C **48**, 1449 (1993).

Figure Captions

FIG. 1

The ground state properties of Na isotopes calculated by the RMF theory without pairing correlation. The top panel shows the proton, matter and charge r.m.s. radii. The open diamonds show the measured matter r.m.s. radius taken from [9]. The bottom panel shows the quadrupole deformation parameters of the proton, matter and neutron density distributions.

FIG. 2

The effective fusion barriers for the s-wave scattering of $^{19,37}\text{Na}$ from ^{208}Pb as functions of the separation distance R between the projectile and target nuclei. The dotted line is the bare potential. The solid and dashed lines have been obtained by respecting the difference between the charge and matter deformations, and by ignoring it, respectively. For each system, the upper and the lower barriers are for the 70.12 and 30.55 degree orientations, respectively.

FIG. 3

Effects of the difference between the nuclear and Coulomb deformations on (a) the fusion excitation functions and (b) the fusion barrier distributions in the $^{19,25,37}\text{Na} + ^{208}\text{Pb}$ reactions. The dotted lines are for the potential model. The solid lines represent the results when the difference of the nuclear(matter) and the Coulomb(charge) deformations is taken into account. The dashed lines have been calculated by ignoring the difference of the charge and matter deformations.

FIG. 4

The sensitivity of (a) the fusion excitation function, and (b) the fusion barrier distribution to the choice of the moment of inertia in the $^{19,37}\text{Na} + ^{208}\text{Pb}$ reactions. The dashed and the solid lines are the same as those in Fig.3. They are compared with the short dashed and the dash-dotted lines obtained by assuming a different value for the moment of inertia in the coupled-channels calculations.

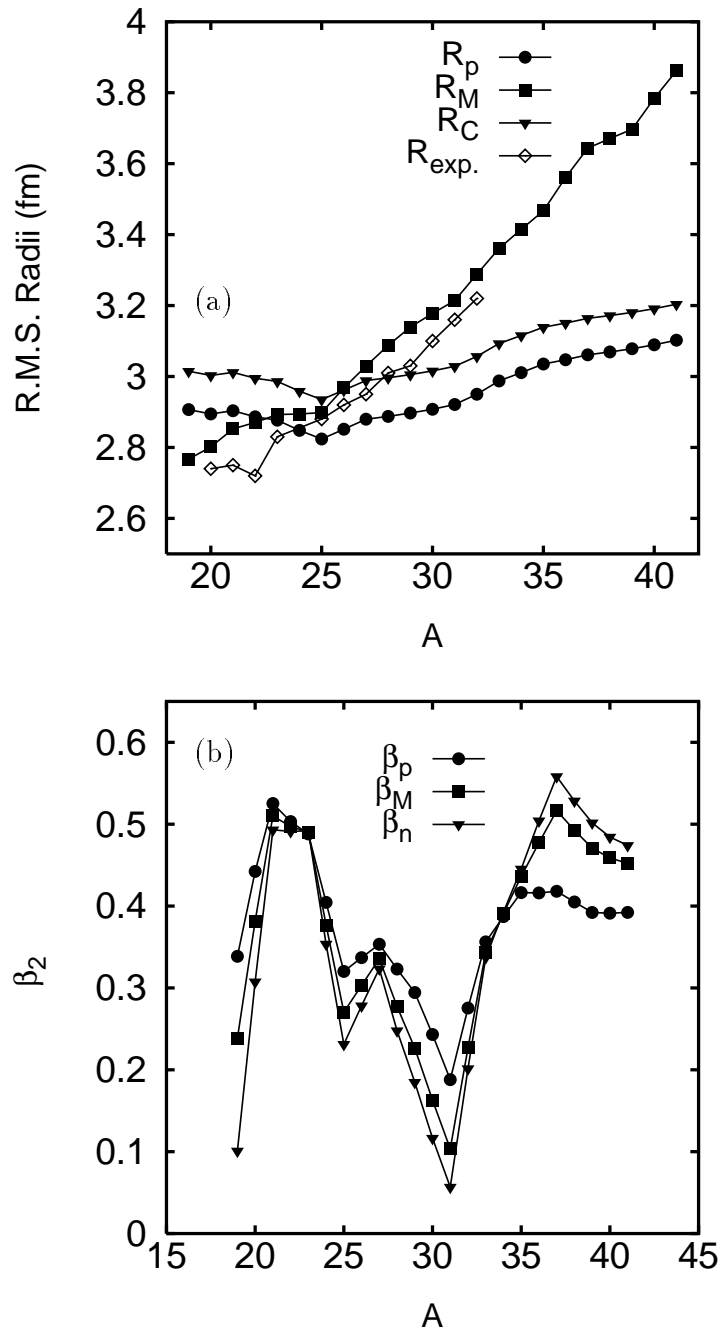


Fig. 1

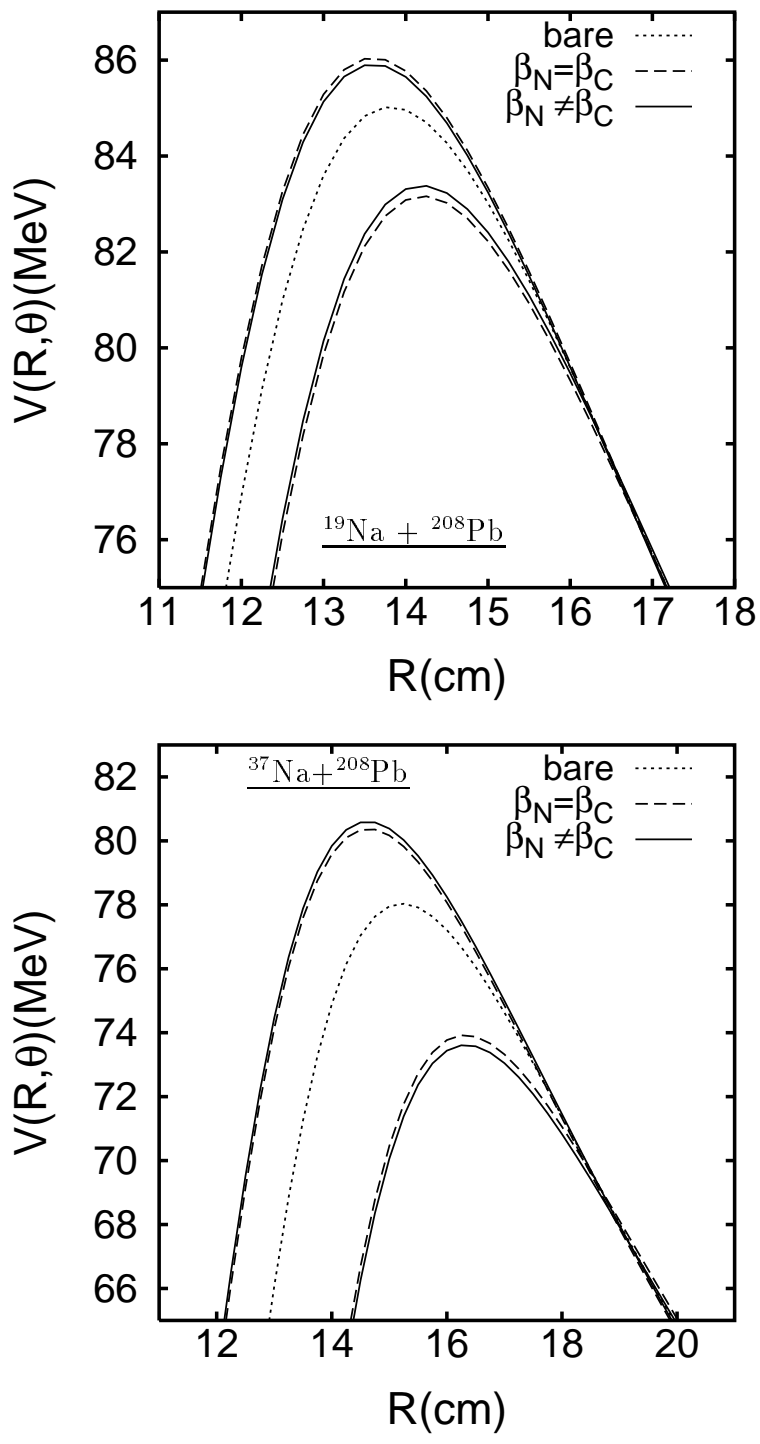


Fig. 2

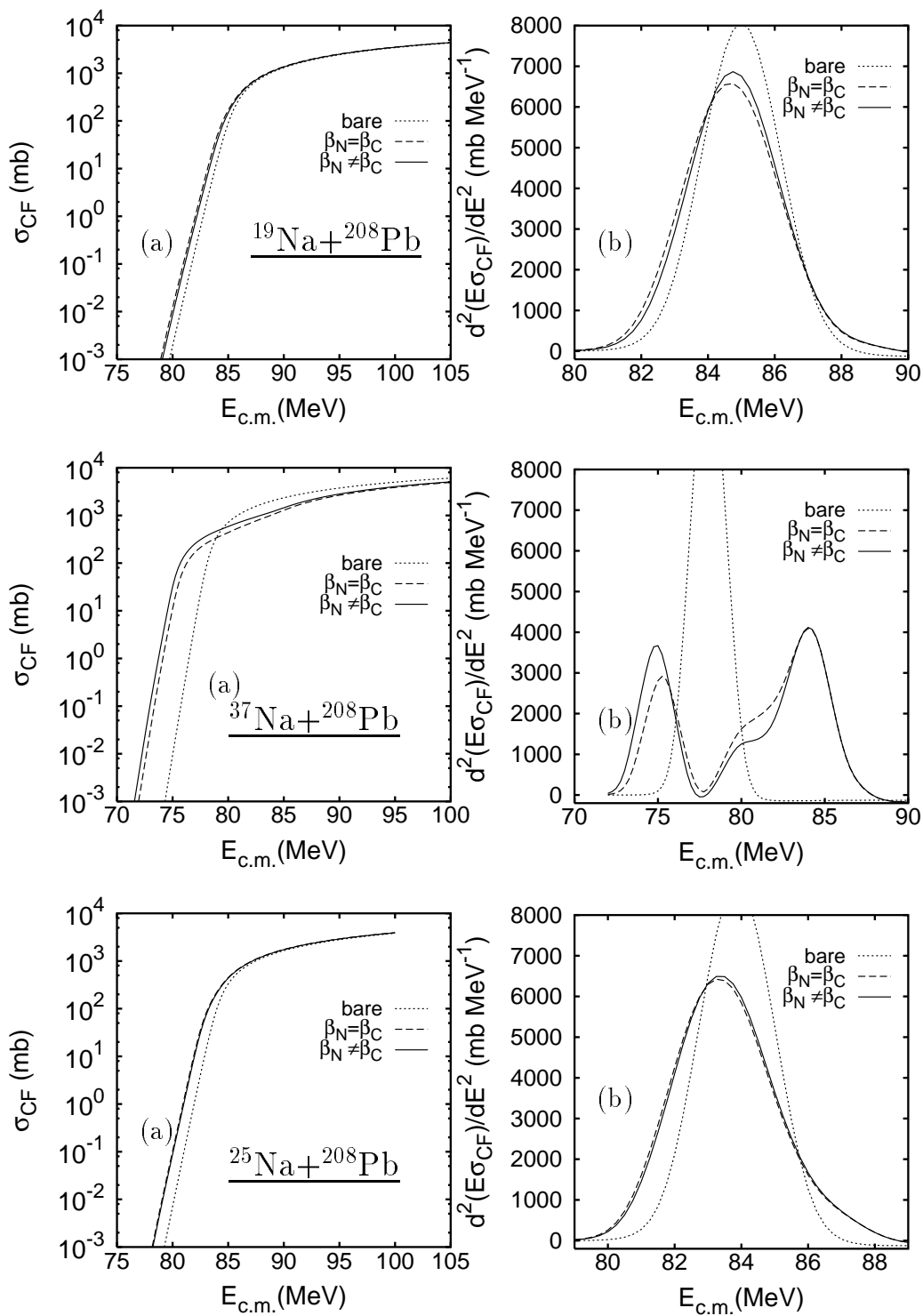


Fig. 3

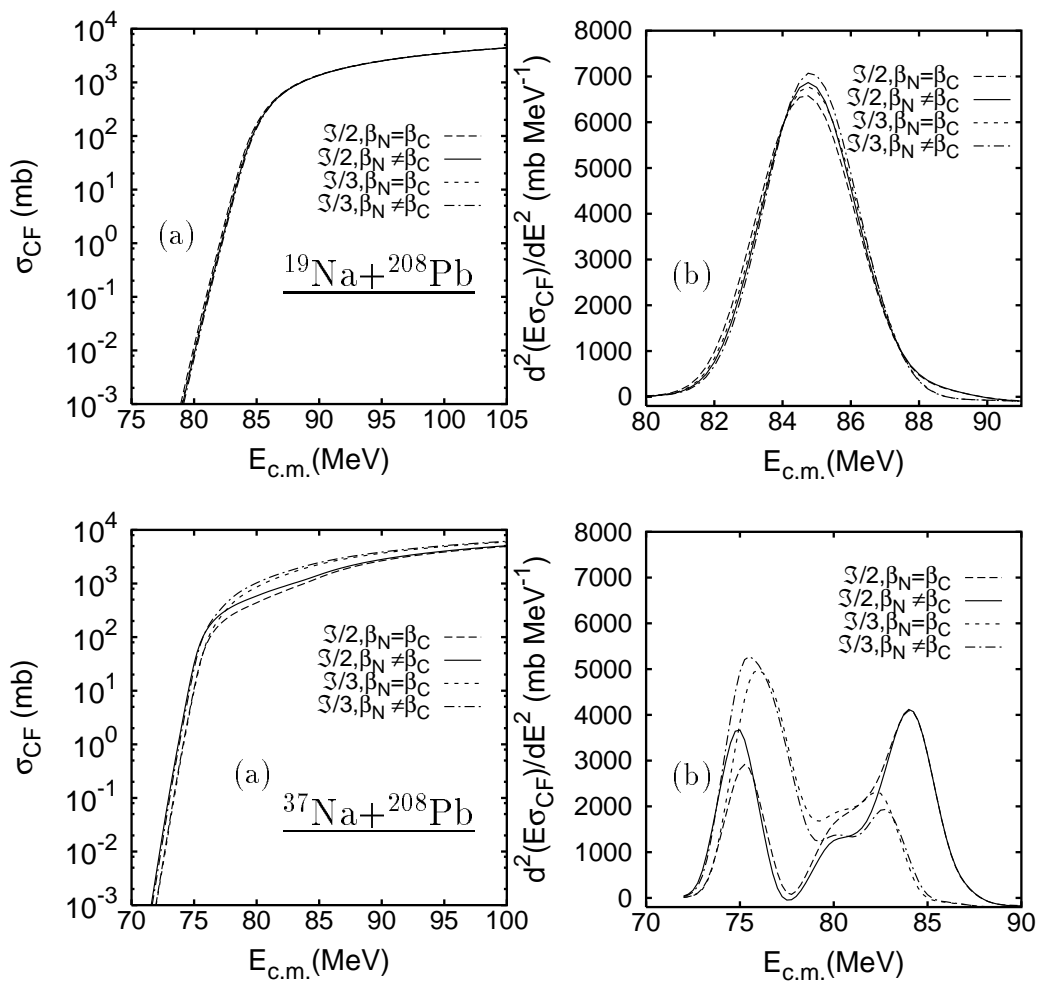


Fig. 4